J|A|C|S
ARTICLES
Published on Web 07/26/2006

Electron Self-Exchange between $Au_{140}^{+/0}$ Nanoparticles Is Faster Than That between $Au_{38}^{+/0}$ in Solid-State, Mixed-Valent Films

Jai-Pil Choi and Royce W. Murray*

Contribution from the Kenan Laboratories of Chemistry, University of North Carolina, Chapel Hill, North Carolina 27599-3290

Received April 19, 2006; E-mail: rwm@unc.edu

Abstract: The well-defined one-electron steps in the voltammetry of solutions of the nanoparticles $Au_{38}(SC2Ph)_{24}$ and $Au_{140}(SC6)_{53}$ (SC2Ph = phenylethanethiolate; SC6 = hexanethiolate) enable preparation of solutions containing, for example, $Au_{38}(SC2Ph)_{24}$ and $Au_{38}(SC2Ph)_{24}^{+}(ClO_4)^{-}$ nanoparticles in known relative proportions. From these solutions can be cast dry, mixed-valent films demonstrably containing the same proportions. Electronic conduction in such mixed-valent films is shown to occur by a bimolecular electron self-exchange reaction at a rate proportional to the concentration product, $[Au_{38}][Au_{38}^{+}]$. The observed $Au_{38}^{+/0}$ rate constant, $\sim 2 \times 10^6$ M^{-1} s^{-1}, is much smaller than that previously observed for $Au_{140}^{+/0}$ films (ca. 4×10^9 M^{-1} s^{-1}; Wuelfing, W. P.; et al. *J. Am. Chem. Soc.* **2000**, *122*, 11465). To our knowledge, this is the first example of a significant size effect in metal nanoparticle electron-transfer dynamics. Thermal activation parameters for the electron-hopping conductivities of the two nanoparticles reveal that the rate difference is mainly caused by energy barriers (E_A) for $Au_{38}^{+/0}$ electron transfers that are larger by ~3-fold than those for $Au_{140}^{+/0}$ electron transfers (ca. 20 vs 7 kJ/mol). Differences in pre-exponential terms in the activation equations for the two nanoparticles are a smaller contributor to the rate constant difference and can be partly ascribed to differences in tunneling distances.

Introduction

A fundamental issue in nanoparticle science is detection and understanding of how physical and chemical properties of a material change with its dimensions—particularly in the nanometer-scale size domain. Nanoparticles of semiconductors such as CdS and CdSe begin to exhibit distinctive size-dependent properties[1−3] in the several nanometer range. This so-called quantum confinement effect has also been found for metal nanoparticles, such as those of gold, but its onset lies at smaller sizes. For example, Chen et al.[4] reported a transition from metal-like double layer capacitive charging to redox-like charging in the voltammetry of solutions of Au nanoparticles containing <200 down to a few tens of Au atoms. The HOMO−LUMO (highest occupied and lowest unoccupied molecular orbitals) energy gap increases with decreasing Au nanoparticle core size, manifesting the quantum confinement effect. Other properties of Au nanoparticles that have been examined as a function of size include mass spectrometry,[5] lifetimes of electronic states,[6] fluorescence,[7] optical spectra,[8] NMR,[9] solubilities in supercritical solution,[10] and catalysis.[11] Reviews by Adams et al.[12] and Daniel and Astruc[13] contain further background information.

Little is known, on the other hand, about how the rates of electron transfers between Au nanoparticles might depend on their sizes. Electron-hopping data for solid films of thiolate-protected Au_{140}, Au_{309}, and Au_{976} nanoparticles uncovered[14,15] no size dependency over this range of Au nanoparticle core sizes. The present work examines smaller nanoparticles in a comparison of electron self-exchange (hopping) rate constants of $Au_{140}(SC6)_{53}^{+/0}$ nanoparticles (abbreviated $Au_{140}^{+/0}$; SC6 = hexanethiolate) with those of $Au_{38}(SC2Ph)_{24}^{+/0}$ nanoparticles (abbreviated $Au_{38}^{+/0}$; SC2Ph = phenylethanethiolate) in their dry, mixed-valent films. The $Au_{140}^{+/0}$ electron-hopping rates have been measured previously.[14] The comparison contrasts a

(1) Heath, J. R. *Science* **1995**, *270*, 1315.
(2) Murray, C. B.; Kagan, C. R.; Bawendi, M. G. *Science* **1995**, *270*, 1335.
(3) Alivisatos, A. P. *Science* **1996**, *271*, 933.
(4) Chen, S.; Ingram, R. S.; Hostetler, M. J.; Pietron, J. J.; Murray, R. W.; Schaaff, T. G.; Khoury, J. T.; Alvarez, M. M.; Whetten, R. L. *Science* **1998**, *280*, 2098.
(5) Negishi, Y.; Nobusada, K.; Tsukuda, T. *J. Am. Chem. Soc.* **2005**, *127*, 5261.
(6) Zhang, J. Z. *Acc. Chem. Res.* **1997**, *30*, 423.
(7) (a) Wang, G.; Huang, T.; Murray, R. W.; Menard, L.; Nuzzo, R. G. *J. Am. Chem. Soc.* **2005**, *127*, 5261. (b) Wang, D.; Imae, T. *J. Am. Chem. Soc.* **2004**, *126*, 13204. (c) Zheng, J.; Zhang, C.; Dickson, R. M. *Phys. Rev. Lett.* **2004**, *93*, 077402. (d) Lee, W. I.; Bae, Y.; Bard, A. J. *J. Am. Chem. Soc.* **2004**, *126*, 8358. (e) Link, S.; Beeby, A.; FitzGerald, S.; El-Sayed, M.; Schaaff, T. G.; Whetten, R. L. *J. Phys. Chem. B* **2002**, *106*, 3410.
(8) Alvarez, M. M.; Khoury, J. T.; Schaaff, T. G.; Shaffigullin, M. N.; Vezmar, I.; Whetten, R. L. *J. Phys. Chem. B* **1997**, *101*, 3706.
(9) (a) Lica, G. C.; Zelakiewicz, B. S.; Tong, Y. Y. *J. Electroanal. Chem.* **2003**, *554−555*, 127. (b) Hostetler, M. J.; Wingate, J.; Zhong, C.-J.; Harris, J. E.; Vachet, R. W.; Clark, M. R.; Londono, J. D.; Green, S. J.; Stokes, J. J.; Wingnal, G. D.; Glish, G. L.; Porter, M. D.; Evans, N. D.; Murray, R. W. *Langmuir* **1998**, *14*, 17. (c) Song, Y.; Harper, A.; Murray, R. W. *Langmuir* **2005**, *21*, 5492. (d) Badia, A.; Demers, L.; Dickinson, L.; Morin, F. G.; Lennox, R. B.; Reven, L. *J. Am. Chem. Soc.* **1997**, *119*, 11104.
(10) Clarke, N. J.; Waters, C.; Johnson, K. A.; Satherley, J.; Schiffrin, D. J. *Langmuir* **2001**, *17*, 6048.
(11) Sau, T. K.; Pal, A.; Pal, T. *J. Phys. Chem. B* **2001**, *105*, 9266.
(12) Adams, D. M.; et al. *J. Phys. Chem. B* **2003**, *107*, 6668.
(13) Daniel, M.-C.; Astruc, D. *Chem. Rev.* **2004**, *104*, 293.
(14) Wuelfing, W. P.; Green, S.; Pietron, J. J.; Cliffel, D. E.; Murray, R. W. *J. Am. Chem. Soc.* **2000**, *122*, 11465.
(15) Wuelfing, W. P.; Murray, R. W. *J. Phys. Chem. B* **2002**, *106*, 3139.

10.1021/ja062736n CCC: $33.50

metal-like quantum capacitor nanoparticle (Au_{140}) with one that is overtly molecule-like (Au_{38}); the latter is found to exhibit a ca. 10^3-fold slower electron-transfer rate constant. To our knowledge, this is the first example of a significant size effect in metal nanoparticle electron-transfer dynamics.

$Au_{38}(SC2Ph)_{24}$ and $Au_{140}(SC6)_{53}$ nanoparticles—or monolayer-protected clusters (MPCs)—can be synthesized[16,17] and isolated from the raw, polydisperse synthetic products in relatively monodisperse forms by solubility differences[17] and annealing.[18] The isolated nanoparticles can be stored in solvent-free form without decomposition or aggregation, and can be redissolved for further characterizations or synthetic manipulations such as ligand or place exchange reactions.[19−23] Au_{38} MPCs differ from Au_{140} MPCs in both core-charging and optical spectroscopic properties. Both nanoparticles have small metal cores (1.1 and 1.6 nm, respectively)[22,24] surrounded by low dielectric ligand shells (phenylethanethiolate and hexanethiolate, respectively). The area-normalized double layer capacitance of Au_{140} is similar to that of a flat, hexanethiolate monolayer-coated gold surface,[25] but the actual Au_{140} surface area is so small that the effective capacitance per nanoparticle (C_{CLU}) is <1 aF. This MPC, as a result, exhibits[26] readily measurable voltage changes ($\Delta V \approx 0.3$ V) upon voltammetric addition or removal of single electrons from its cores; i.e., it is a quantum (double layer) capacitor. Au_{140} is regarded as a metal-like nanoparticle since no energy gap (gap between highest occupied and lowest unoccupied molecular orbitals) has been detected. Au_{38} MPCs, in contrast, display a substantial energy gap; in electrochemical context there is a 1.6 V difference between[27] the formal potentials of the $Au_{38}^{+/0}$ and $Au_{38}^{0/-}$ couples. Indeed, the voltammetric charging of Au_{38} MPC cores is similar to redox transformations of other small metal cluster compounds, such as the platinum carbonyl,[28] $[Pt_{24}(CO)_{30}]$. Differences between Au_{140} and Au_{38} are also evident in their UV−vis absorption spectra, where Au_{140} shows a relatively featureless decrease in absorbance from high to low energy, while Au_{38} exhibits discrete spectral features riding atop the absorbance decrease.[4,27]

Measurements of electron and ion transport properties through films of metal nanoparticles are relevant to their practical applications in sensors[29] and in electronic devices with nanoscale features.[30] Despite its potential importance, this research area has not been explored extensively. To thoroughly understand electron transport, one must additionally consider the molecularity of the electron-hopping process, i.e., the role of the carrier population or, said differently, the role of the state of mixed valency of the nanoparticle cores. By mixed-valent MPC films, we mean films containing experimentally defined mixtures of core charge states. Solid-state, mixed-valent Au_{140} nanoparticle films—as revealed by their electronic conductivities—have been shown[14] to depend on their charge state composition according to a bimolecular rate law for the self-exchange reaction

$$Au_{140}^{0} + Au_{140}^{+} \xrightarrow{k_{EX}} Au_{140}^{+} + Au_{140}^{0} \qquad (1)$$

where k_{EX} is the bimolecular rate constant ($M^{-1}\ s^{-1}$). The rate of reaction 1, and the corresponding electronic conductivity (σ_{EL}) of the MPC films, are largest for equal populations of Au_{140}^{0} and Au_{140}^{+}. Mixed valency can, of course, also be generated by thermal excitation, so that (for example), to a small extent, by disproportionation, Au_{140}^{+} and Au_{140}^{-} appear in a nominally neutral Au_{140}^{0} film. Thermal excitation (i.e., disproportionation) is the dominant source of mixed valency in films of much larger nanoparticles but is unimportant when a significant extent of mixed valency has been otherwise (chemically) introduced, or when the potential spacing between charge state couples is significant, as with Au_{140} and, especially, Au_{38}.

Previous reports of electron transport properties in films of gold nanoparticles[14,15,22,29,31] have been limited to larger, metal-like gold cores. This paper deals with two nanoparticles that span the metal-like to molecule-like boundary. We find that the electronic conduction properties of mixed-valent Au_{38} MPC films again follow a bimolecular rate law but exhibit a rate constant much smaller than that of the Au_{140} MPCs. The origin of the rate difference is established to lie mainly in differences in the thermal activation energy barriers.

Experimental Section

Chemicals. Hydrogen tetrachloroaurate(III) trihydrate ($HAuCl_4 \cdot 3H_2O$) was synthesized by a literature method.[32,33] Phenylethanethiol ($PhCH_2CH_2SH$, 98%, or PhC2SH), sodium borohydride ($NaBH_4$, 99%), cerium(IV) sulfate ($Ce(SO_4)_2$), tetraoctylammonium bromide (Oct_4NBr, 98%), sodium perchlorate ($NaClO_4$, 99.9%), and tetrabutylammonium perchlorate (Bu_4NClO_4, ≥99.0%) were purchased from Aldrich or Fluka (Milwaukee, WI). Toluene, methanol (optima grade), acetonitrile (CH_3CN, optima grade), and dichloromethane (CH_2Cl_2, optima grade) were obtained from Fisher Scientific (Suwanee, GA). Ethanol (absolute, i.e., 200 proof) was purchased from Aaper Alcohol and Chemical Co. (Shelbyville, KY). All chemicals were used without further purification. Deionized water (>18 MΩ) was prepared with a Millipore Nanopure water purification system.

Au_{38} Nanoparticle Syntheses. $Au_{38}(SC2Ph)_{24}$ was synthesized as reported[17] previously. The synthesis is summarized in the Supporting Information.

Chemical Charging of Au_{38} Nanoparticles. Mixed-valent charging of gold nanoparticles was conducted[14] with the oxidant Ce(IV). An aqueous solution (10 mL) of 5 mM $Ce(SO_4)_2$ and 0.1 M $NaClO_4$ was

(16) Brust, M.; Walker, M.; Bethell, D.; Schiffrin, D. J.; Whyman, R. *J. Chem. Soc., Chem. Commun.* **1994**, 801.
(17) Donkers, R. L.; Lee, D.; Murray, R. W. *Langmuir* **2004**, *20*, 1945.
(18) Hicks, J. F.; Miles, D. T.; Murray, R. W. *J. Am. Chem. Soc.* **2002**, *124*, 13322.
(19) Wuelfing, W. P.; Gross, S. M.; Miles, D. T.; Murray, R. W. *J. Am. Chem. Soc.* **1998**, *120*, 12696.
(20) Hostetler, M. J.; Templeton, A. C.; Murray, R. W. *Langmuir* **1999**, *15*, 3782.
(21) Song, Y.; Murray, R. W. *J. Am. Chem. Soc.* **2002**, *124*, 7096.
(22) Lee, D.; Donkers, R. L.; DeSimone, J. M.; Murray, R. W. *J. Am. Chem. Soc.* **2003**, *125*, 1182.
(23) Song, Y.; Huang, T.; Murray, R. W. *J. Am. Chem. Soc.* **2003**, *125*, 11694.
(24) Wuelfing, W. P.; Green, S. J.; Pietron, J. J.; Cliffel, D. F.; Murray, R. W. *J. Am. Chem. Soc.* **2000**, *122*, 11465.
(25) Porter, M. D.; Bright, T. B.; Allara, D. L.; Chidsey, C. E. D. *J. Am. Chem. Soc.* **1987**, *109*, 3559.
(26) Chen, S.; Murray, R. W.; Feldberg, S. W. *J. Phys. Chem. B* **1998**, *102*, 9898.
(27) Lee, D.; Donkers, R. L.; Wang, G.; Harper, A. S.; Murray, R. W. *J. Am. Chem. Soc.* **2004**, *126*, 6193.
(28) Roth, J. D.; Lewis, G. J.; Safford, L. K.; Jiang, X.; Dahl, L. F.; Weaver, M. J. *J. Am. Chem. Soc.* **1992**, *114*, 6159.
(29) Zamborini, F. P.; Leopold, M. C.; Hicks, J. F.; Kulesza, P. J.; Malik, M. A.; Murray, R. W. *J. Am. Chem. Soc.* **2002**, *124*, 8958.
(30) Joachim, C.; Gimzewski, J. K.; Aviram, A. *Nature* **2000**, *408*, 541.
(31) (a) Brust, M.; Bethell, D.; Kiely, C. J.; Schiffrin, D. J. *Langmuir* **1998**, *14*, 5425. (b) Pietron, J. J.; Hicks, J. F.; Murray, R. W. *J. Am. Chem. Soc.* **1999**, *121*, 5565. (c) Hicks, J. F.; Zamborini, F. P.; Osisek, A. J.; Murray, R. W. *J. Am. Chem. Soc.* **2001**, *123*, 7048. (d) Schmid, G.; Corain, B. *Eur. J. Inorg. Chem.* **2003**, *2003*, 3081. (e) Leopold, M. C.; Donkers, R. L.; Georganopoulou, D.; Fisher, M.; Zamborini, F. P.; Murray, R. W. *Faraday Discuss.* **2004**, *125*, 63. (f) Wessels, J. M.; Nothofer, H.-G.; Ford, W. E.; Wrochem, F. V.; Scholz, F.; Vossmeyer, T.; Schroedter, A.; Weller, H.; Yasuda, A. *J. Am. Chem. Soc.* **2004**, *126*, 3349.
(32) *Handbook of Preparative Inorganic Chemistry*; Brauer, G., Ed.; Academic Press: New York, 1965; p 1054.
(33) Block, B. P. *Inorg. Synth.* **1953**, *4*, 14.

vigorously stirred with a CH_2Cl_2 solution (5 mL) of ~0.1 mM Au_{38} and 0.05 M Bu_4NClO_4, for various times. The reaction time determines the proportions of Au_{38}^0 and Au_{38}^+ in the CH_2Cl_2 product solution. Solutions containing Au_{38}^{2+} were produced in a few cases. The upper aqueous solution was then decanted and the CH_2Cl_2 removed at room temperature under reduced pressure. The mixed-valent MPCs were washed five times with 10 mL of methanol to remove Bu_4NClO_4. The counterion of the positively charged Au_{38} MPCs is assumed to be perchlorate. The mixed-valent MPCs were stored in dry form, in which the charges states are stable for weeks or longer.

Electrochemical Measurements. Cyclic voltammetry (CV), differential pulse voltammetry (DPV), and rest potential (E_R) measurements of MPC solutions (in CH_2Cl_2) were conducted with a CHI 660 electrochemical workstation (Austin, TX). The conventional electrochemical cell contained 2 mm diameter Pt working electrode, Pt coil counter electrode, and Ag/Ag^+ (10 mM $AgNO_3$ in CH_3CN) reference electrodes. The formal potential of the ferrocene couple (Fc/Fc^+) was +0.22 V vs this reference electrode.

Film Preparation on Interdigitated Array Electrodes and Electronic Conductivity (σ_{EL}) Measurements. Gold interdigitated array (IDA) electrodes purchased from Abtech Scientific (Richmond, VA) had 50 interdigitated fingers, each finger being 20 μm wide, 3 mm long, 180 nm high, and spaced 20 μm apart. Films of gold MPCs were drop-cast onto the IDAs from concentrated solutions (ca. 10 mg in 0.1 mL of CH_2Cl_2) of the mixed-valent nanoparticles. The IDA films were dried in a vacuum oven at room temperature for 24 h. The film thickness (~1 μm, much greater than the finger height) was measured by stylus profilometry (Tencor Alpha-Step 100). The total concentration of MPCs in a dried Au_{38} film was estimated as 0.17 M on the basis of UV−vis absorption spectra of three different Au_{38} films (on glass) of 450−740 nm thickness. The film-coated IDA was mounted on a temperature-controlled stage in a vacuum chamber and kept there under vacuum for 1 h to ensure dryness.

The electronic conductivities of mixed-valent MPC films were measured from the slopes of (linear) current−potential plots obtained by scanning the bias potential across the IDA fingers between ±1 V (initial and final voltage is 0 V) at 100 mV/s, at temperatures between −60 and 30 °C, starting at −60 °C and warming in 10 °C increments, allowing 20 min for equilibration at each temperature. The electronic conductivity σ_{EL} was calculated from the $\Delta i/\Delta E$ slopes,

$$\sigma_{EL} = \frac{d\Delta i}{A_{TOTAL}\Delta E} \quad (2)$$

where d is the IDA gap, and A_{TOTAL} is defined as the area of the walls of facing parallel plate finger electrodes (A_{FINGER}) of height equal to the MPC film thickness (1 μm) and of length equal to the finger length times ($N - 1$), where N is the number of IDA fingers. The ratio d/A_{TOTAL} comprises the geometric cell constant (C_{CELL}, cm^{-1}). Based on the above, $C_{CELL} = 1.36\ cm^{-1}$.

In previous work on Au_{140} films,[14,15,29,31e] the MPC films were also 1 μm thick, but the calculation of the IDA C_{CELL} (6.25 cm^{-1}) was based on the IDA finger height rather than on the film height. To compare the previous[14] Au_{140} data to the present Au_{38} results, the Au_{140} conductivities were recalculated using the cell constant of 1.36 cm^{-1}. A discussion of different models for evaluating cell constants is given in the Supporting Information.

Results and Discussion

Establishing Charge State Compositions of Mixed-Valent $Au_{38}^{+/0}$ Films. The room-temperature voltammetry of $Au_{38}(SC2Ph)_{24}$ displays[22,27] single-electron oxidation steps up to Au_{38}^{3+} and one reduction step. The first two oxidations—the $Au_{38}^{+/0}$ and $Au_{38}^{2+/+}$ couples—are chemically reversible on the voltammetric time scale (Figure 1), whereas Au_{38}^{3+} and Au_{38}^- have lower stability (Figure S3, Supporting Information).

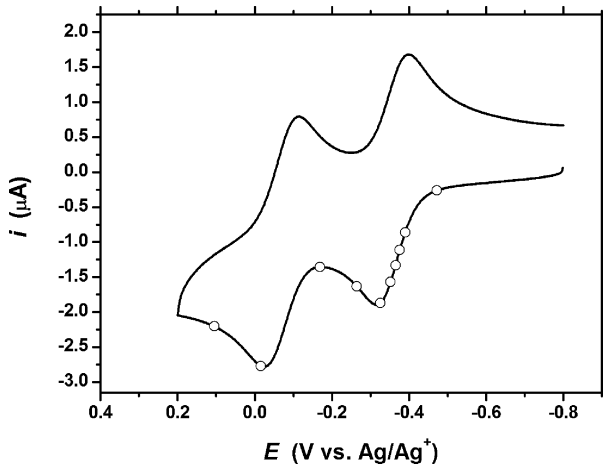

Figure 1. Cyclic voltammetry (CV, 2 mm diameter Pt working electrode, 100 mV/s) of 0.1 mM $Au_{38}(SC2Ph)_{24}$ in CH_2Cl_2 containing 0.1 M Bu_4NClO_4. The open circles on the CV trace represent solution rest potentials of chemically prepared mixed-valent solutions.

Table 1. Rest Potential (E_R) and Charge State Composition of Mixed-Valent Au_{38} Nanoparticles Prepared by Ce(IV) Oxidation

E_R (V vs Ag/Ag^+)	t_{RXN} (min)[a]	Au_{38}^0 (%)[b]	Au_{38}^+ (%)[b]	Au_{38}^{2+} (%)[b]
−0.47	0	99	1	
−0.39	0.5	76	24	
−0.38	1	65	34	
−0.37	1.5	55	45	
−0.35	2	42	58	
−0.33	4	21	79	
−0.27	6	2	98	
−0.17	10	0	100	
0.11	180		0	100

[a] Reaction time allowed for chemical charging by Ce(IV). [b] Calculated by eq 3 and $E^{\circ\prime} = -0.36$ and −0.07 V.

To be best assured of stability of our mixed-valent mixtures, we focused on preparing $Au_{38}^{+/0}$ films. One Au_{38}^{2+} film was explored.

The mixed-valent Au_{38} samples were prepared by a two-phase oxidation, using aqueous $Ce(SO_4)_2$ as the oxidant, as previously described.[14] The charged MPCs were isolated from the reaction solution, dried, and stored. The dried solids are stable; the rest potentials of solutions prepared from them are the same, within a few millivolts, as those of the original mixed-valent MPC solutions. The rest potentials reflect the relative concentrations of Au_{38}^+ and Au_{38}^0 MPC charge states present, as given by the Nernst equation[34] (which mixed-valent thiolate-protected Au MPC solutions have been shown[31b] to obey):

$$E_R - E^{\circ\prime} = 0.059 \log\frac{[Au_{38}^{Z+1}]}{[Au_{38}^{Z}]} \quad (3)$$

where $E^{\circ\prime}$ is the formal potential, and the charge number Z is 0 or 1. $E^{\circ\prime} = -0.36$ and −0.07 V vs Ag/Ag^+ for the $Au_{38}^{0/+}$ and $Au_{38}^{+/2+}$ couples, respectively, from Figure 1. Rest potentials of prepared mixed-valent solutions are indicated as open circles in Figure 1, and are listed in Table 1.

Solid-state, mixed-valent MPC films on IDAs were prepared by drop-casting from solutions of known E_R. The total Au_{38}

(34) Bard, A. J.; Faulkner, L. R. *Electrochemical Methods: Fundamentals and Applications*, 2nd ed.; Wiley and Sons: New York, 2001.

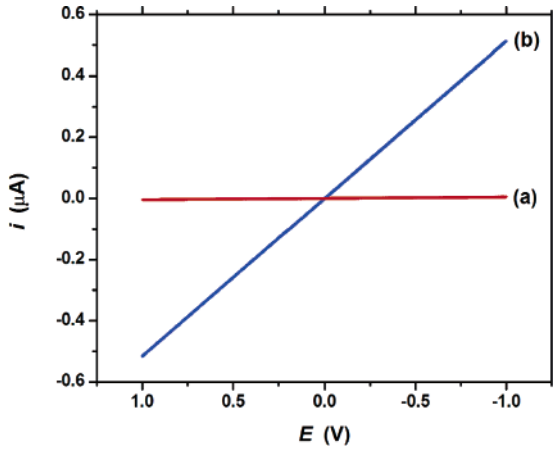

Figure 2. Current−potential ($i-E$) responses of Au_{38} films containing (a) 99% Au_{38}^0 and 1% Au_{38}^+ and (b) 42% Au_{38}^0 and 58% Au_{38}^+ at 100 mV/s and 30 °C. Measurements were performed on films on IDA electrodes (C_{CELL} = 1.36 cm^{-1}).

MPC concentration in such films is 0.17 M, as estimated from UV−vis absorbance (at 695 nm, where ϵ = 13 060 M^{-1} cm^{-1}) of films of known thickness (see Experimental Section and Figure S4, Supporting Information). The ratios and actual [Au_{38}^+] and [Au_{38}^0] concentrations in Table 1 are calculated from the above information.

Figure 1 and Table 1 show that the E_R of as-prepared Au_{38} nanoparticles (−0.472 V) is well negative of the $Au_{38}^{0/+}$ formal potential; such solutions are mainly Au_{38}^0. The E_R of Au_{38} solutions reacted with Ce(IV) becomes gradually more positive with longer reaction times. The charging reaction is rather slow, even with a 50-fold excess of Ce(IV), and it was difficult to reproduce any given charge state, presumably because of variations in the effectiveness of heterogeneous contact between the stirred water/organic reaction phases.

Measurements of σ_{EL} and of Self-Exchange Rate Constants. The electronic conductivities σ_{EL} of Au_{38} nanoparticle films on IDA electrodes were measured as described in the Experimental Section and Supporting Information. As discussed previously,[14] to accurately obtain an electric field-driven electron-hopping conductivity, it is essential to avoid electrolysis reactions at the electrode/film interface; i.e., ion mobilities within the film must be insignificant on the experimental time scale. Electrolysis is signaled by hysteresis effects in current−potential ($i-E$) plots. Figure 2 shows that current−potential responses are linear (ohmic) and lack any hysteresis, and further, Figure S5 (Supporting Information) shows that $i-E$ plots are independent of potential scan rate.

As noted in the Introduction, electron transport in a mixed-valent $Au_{38}^{+/0}$ MPC film is expected to occur by bimolecular self-exchanges analogous to eq 1, at a rate proportional to the electronic conductivity:

$$Au_{38}^{\ 0} + Au_{38}^{\ +} \xrightarrow{k_{EX}} Au_{38}^{\ +} + Au_{38}^{\ 0} \qquad (4)$$

The reaction's bimolecularity leads to the expectation that σ_{EL} depends on the relative proportions of Au_{38}^0 and Au_{38}^+ charge states in the film, notably that σ_{EL} should decrease at low degrees of mixed valency (i.e., high proportions of Au_{38}^0 or Au_{38}^+) and become maximized at 1:1 proportions. Table 2 and Figure 3 show that σ_{EL} indeed behaves in this manner for the $Au_{38}^{+/0}$ mixtures. Results are also given there for the previously determined mixed-valent Au_{140} films. Figure 3, black and blue dots, presents the conductivity data as a function of the percentage of Au^+ charge state. The red dotted lines are fits of a second-order rate law of electron hopping between electronically localized sites to the conductivity data; the fits are reasonable.

Table 2. Electronic Conductivities (σ_{EL}) and Self-Exchange Rate Constants (k_{EX}) for Au_{38} and Au_{140} Nanoparticles

	charge state composition in film (%)			
nanoparticle	0	1+	σ_{EL} (Ω^{-1} cm^{-1})	k_{EX} (M^{-1} s^{-1})
Au_{38}	99	1	6.1×10^{-9} [b]	7×10^5
	76	24	$1.9. \times 10^{-7}$	1×10^6
	65	34	2.7×10^{-7}	2×10^6
	55	45	4.8×10^{-7}	2×10^6
	42	58	7.0×10^{-7}	2×10^6
	21	79	3.2×10^{-7}	2×10^6
	2	98	1.2×10^{-8}	7×10^5
Au_{140}[a]	99	1	2.9×10^{-5}	6×10^9
	98	2	4.0×10^{-5}	5×10^9
	97	3	4.8×10^{-5}	3×10^9
	93	7	7.2×10^{-5}	3×10^9
	81	19	2.2×10^{-4}	3×10^9
	3	97	6.4×10^{-5}	6×10^9

[a] Taken from ref 14 and recalculated using C_{CELL} = 1.36 cm^{-1}. [b] Average of three different films with the same charge-state composition (standard deviation = $\pm 0.6 \times 10^{-9}$ Ω^{-1} cm^{-1}).

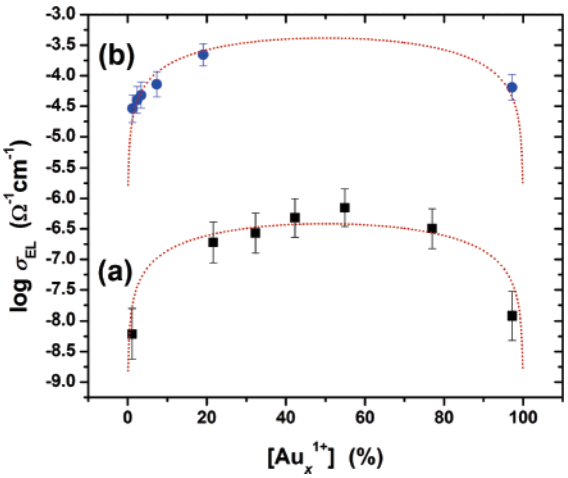

Figure 3. Effect of the concentration, [Au_x^+] (x = 38 or 140), on σ_{EL}. (a) Mixed-valent Au_{38} MPCs; (b) mixed-valent Au_{140} MPCs. Estimated error bars are ±10%. The red curves are σ_{EL} values simulated for a bimolecular reaction with rate constants 1.5×10^6 M^{-1} s^{-1} for Au_{38} and 4.3×10^9 M^{-1} s^{-1} for Au_{140}.

In mixed-valent $Au_{38}^{+/0}$ films in which either the Au_{38}^0 or Au_{38}^+ state is dominant, the conductivities are about 20-fold smaller than the maximum conductivity (Figure 3) at a 1:1 molar ratio. These results are in contrast to those obtained in doped semiconductors, where electronic conductivity continues to increase with increased levels of introduced carriers and occurs via an extended band structure.

The electronic conductivities are converted to electron self-exchange rate constants (k_{EX}) on the basis of the usual (approximate) cubic lattice model of film structure,[14,15]

$$k_{EX} = \frac{6RT\sigma_{EL}}{10^{-3}F^2\delta^2[Au_{38}^{\ 0}][Au_{38}^{\ +}]} \qquad (5)$$

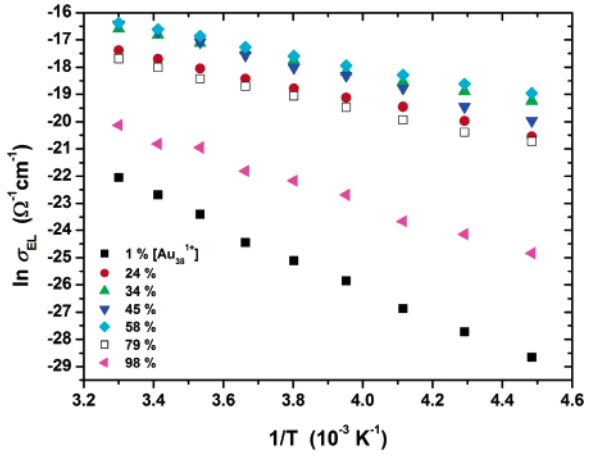

Figure 4. Thermal activation plot of dry mixed-valent Au_{38} MPC films containing the indicated proportions of Au_{38}^+.

where the center-to-center electron-hopping distance is

$$\delta = 2(r_{core} + l_{app}) = 2\sqrt[3]{\frac{0.7}{10^{-3}(4/3)}\pi C_{FILM} N_A} \qquad (6)$$

in which 0.7 is a hexagonal packing fill factor, r_{core} is the core radius, l_{app} is the apparent ligand length, C_{FILM} is the film concentration (0.17 M), and N_A is Avogadro's number. δ = 2.4 nm based on C_{FILM}, and from eq 6, l_{APP} of the Au_{38} phenylethanethiolate ligand is 0.6 nm. This latter length is close to that of the fully extended ligand (0.68 nm),[35] suggesting a minor extent of interdigitation of ligands of adjacent MPCs. k_{EX} values calculated from eq 6 are summarized in Table 2. k_{EX} is relatively constant (except at the lowest and highest percentages of Au_{38}^+), as anticipated for a bimolecular reaction. The results at the lowest and highest percentages of Au_{38}^+ will be discussed later.

The most significant result of the Table 2 and Figure 3 comparisons is that the bimolecular rate constants for the $Au_{140}^{+/0}$ MPC self-exchange are $\sim 2 \times 10^3$-fold larger than those for $Au_{38}^{+/0}$. *This is the first experimental observation of a size-dependent difference in electron-transfer rates for metal-based nanoparticles.*

Thermal Energy Barriers (E_A) for Electron Hopping. Why does the smaller nanoparticle display slower electron self-exchanges? The thermally activated electron transfers in Au nanoparticle films follow[14] the general relation

$$k_{EX} = A \exp[-E_A/RT] \qquad (7)$$

The temperature dependences of the electronic conductivity of the seven different mixed-valent Au_{38} films in Table 1, plotted in Figure 4 according to eq 7, are linear over a 90 °C range (−60° to 30 °C). The resulting activation energy barriers E_A and pre-exponential terms A are listed in Table 3. Again, excluding the results at the lowest and highest percentages of Au_{38}^+ (discussed later), the mixed-valent Au_{38} films give consistent values of E_A; the energy barrier is independent of charge state, with an average value of 20 ± 1 kJ/mol (e.g., 0.21 eV).[36]

(35) Calculated by a modeling software, Gaussian.
(36) E_A's of the films of 1% Au_{38}^+ and 97% Au_{38}^+ were excluded in calculation of the average.

Table 3. Activation Energy Barriers (E_A) and Pre-exponential Terms (A) of Solid-State, Mixed-Valent Au_{38} Nanoparticle Films

	charge state composition in film (%)			
nanoparticle	0	1+	E_A (kJ/mol)	A $(M^{-1}\,s^{-1})^b$
Au_{38}	99	1	46.7	4×10^{12}
	76	24	21.6	3×10^8
	65	34	19.6	1×10^8
	55	45	20.3	3×10^8
	42	58	19.2	3×10^8
	21	79	21.7	5×10^8
	2	98	33.0	1×10^{10}
Au_{140}[a]	99	1	7.7	7×10^9
	98	2	6.8	3×10^9
	97	3	6.0	2×10^9
	93	7	7.4	3×10^9
	81	19	5.6	2×10^9
	3	97	14.8	(1×10^{34})

[a] Taken from ref 14. [b] From intercepts of Figure 4.

The previously determined[14] energy barrier results for Au_{140} MPCs are also given in Table 3. Excluding the points at the lowest and highest percentages of Au_{140}^+, the average energy barrier for Au_{140} is 6.7 ± 0.8 kJ/mol (i.e., 0.07 eV). These energy barrier data were obtained from electronic conductivity results, but they also represent the energy barriers for electron transfers. The results show that *barriers for Au_{38} are 3-fold larger than those of Au_{140}*; this large energy barrier difference is the primary source of the difference in Au_{140} and Au_{38} self-exchange rate constants described in Table 2. The 3-fold energy barrier difference amounts to a 190-fold difference in rate constant, a substantial part of the observed 2×10^3-fold difference.

Table 3 also gives results derived from Figure 4 for the pre-exponential term A, which in self-exchange rate constant units are, for Au_{38} and Au_{140}, $(3.0 \pm 1.4) \times 10^8$ and $(2.5 \pm 0.6) \times 10^9$ M^{-1} s^{-1}. The difference is 9-fold (again excluding results at the highest and lowest mixed valencies). Combined with the 190-fold rate difference attributable to the activation energy barrier difference, the A term result leads to a prediction of a rate constant difference between Au_{38} and Au_{140} electron hopping of 1.7×10^3-fold, in excellent agreement with the rate measurements and satisfactorily accounting for the rate results in the context of eq 7.

Turning next to the possible origins of the differences in A and E_A parameters for Au_{38} and Au_{140} MPCs, we consider first factors that can influence the magnitude of A; these involve, variously expressed, electron tunneling barriers, the adiabaticity of the electron transfers, the density of electronic states of the reactants, nuclear and electronic frequency factors, and entropy of activation. The last factor, entropy of activation, should be zero since the electron self-exchange is symmetrical.[37] Previous results on electron transfers between MPCs coated with alkanethiolate chains,[14,29,31e] and between related redox self-assembled monolayers on planar Au surfaces,[25,38] have been consistent with electron transfer by electron tunneling between the Au_{38} and Au_{140} cores. The tunneling involves nonbonding contacts, which are known to offer efficient tunneling pathways.[15,39,40] While the modeled extended chain lengths of the

(37) (a) Sutin, N.; Weaver, M. J.; Yee, E. L. *Inorg. Chem.* **1980**, *19*, 1096. (b) Marcus, R. A.; Sutin, N. *Biochim. Biophys. Acta* **1985**, *811*, 265. (c) Marcus, R. A. *Angew. Chem., Int. Ed. Engl.* **1993**, *32*, 1111.
(38) Smalley, J. F.; Feldberg, S. W.; Chidsey, C. E. D.; Linford, M. R.; Newton, M. D.; Liu, Y.-P. *J. Phys. Chem.* **1995**, *99*, 13141.

$-S(CH_2)_2Ph$ and $-S(CH_2)_5CH_3$ ligands are similar, 0.68 and 0.77 nm, respectively, the alkanethiolate chains between neighbor Au_{140} MPC cores are intercalated[15] to a greater extent. Based on density measurements on MPC samples, the core edge−edge separations are not twice the extended chain lengths; instead, $2l_{APP} = 0.92$ nm for Au_{140} and 1.2 nm for Au_{38} MPCs, which leaves a 0.28 nm difference in tunneling distance. Assuming an electron coupling factor[38] of $\beta \approx 1.0$/Å suggests a potentially 16-fold larger tunneling rate for Au_{140} based on distance alone. This difference is comparable to the ∼9-fold difference for *A* in Table 3. As a caveat, however, we must note that the two nanoparticles have different monolayer shells, i.e., $-S(CH_2)_2Ph$ for Au_{38} and $-S(CH_2)_5CH_3$ for Au_{140}, and that studies[15] of mixed alkane/arene MPC monolayers (like $-S(CH_2)_2Ph$) show that the aromatic components are considerably more transmissive. This would lessen the anticipated tunneling distance factor.

At the outset of this study, we were intrigued that differences in densities of electronic states might exert a strong influence on rate constants for these two nanoparticles. The Au_{38} nanoparticles are molecule-like with discrete molecular orbital energies, whereas Au_{140} nanoparticles possess a more-or-less continuous density of electronic states. The observed difference in the pre-exponential *A* terms for the two nanoparticles may be due, in part, to differences in densities of electronic states for these two nanoparticles,[41−43] but they are clearly not the most prominent factor; E_A is.

Analysis of the origin of the 3-fold difference in E_A proved to be more problematical. Examination of Marcus theory[37,44] expressions for free energy of activation (ΔG^*) in terms of reorganizational factors adds a few insights into this issue. We have previously employed[45] this dielectric continuum model as a rough basis for anticipating outer-sphere energy barriers for electron hopping in semi-solid mixed-valent materials, taking the chemical medium attached to the redox sites as, crudely, constituting its "solvent". The classical outer-sphere energy barrier relation is

$$\Delta G^* = \frac{\lambda}{4}\left(1 + \frac{\Delta G^\circ}{\lambda}\right)^2 \qquad (8)$$

where $\lambda = \lambda_o + \lambda_i$, the sum of outer-sphere (solvent polarization) and inner-sphere (vibrational) reorganizational energies. For the reaction free energy $\Delta G^\circ = 0$ (self-exchange) and assuming $\lambda_i = 0$,

$$\Delta G^* = \frac{\lambda}{4} = \frac{e^2 N_A}{16\pi\epsilon_o}\left(\frac{1}{2r_1} + \frac{1}{2r_2} - \frac{1}{r_{12}}\right)\left(\frac{1}{\epsilon_{op}} - \frac{1}{\epsilon_s}\right) \qquad (9)$$

where *e* is the electronic charge transferred, r_1 and r_2 are the radii of reactants, r_{12} is the center-to-center separation distance at the transition state, ϵ_{op} is the optical dielectric constant, ϵ_s is the static dielectric constant, and ϵ_o is the dielectric constant in a vacuum. ΔG^* can be equated with the energy barrier E_A since the entropy of activation for a symmetrical self-exchange is zero. This relation shows that ΔG^* is expected to decrease for larger reactants in lower dielectric environments, consistent with the actual results of quite large electron-transfer rates (Table 2). In using this relation, we consider the MPC core radii as the relevant reactant radii and the MPC monolayer as providing the dielectric environment. Based on $2r_1 = 2r_2 = 1.1$ and 1.6 nm, $r_{12} = 2.3$ and 2.52 nm, $\epsilon_{op} = 2.4$ and 2.1 (square of refractive index of the free thiols), and $\epsilon_s = 3.9$[15] and 3.0[18] for Au_{38} and Au_{140} MPCs, respectively, eq 9 predicts outer-sphere ΔG^* values of 7.7 and 4.2 kJ/mol, respectively. These estimates miss the experimental result by ca. 12 and 2.5 kJ/mol, respectively. The discrepancy for the Au_{38} nanoparticle is obviously much larger. The prediction of a slower Au_{38} rate on account of the dimension and dielectric parameters of eq 9 is in the correct direction and qualitatively explains some, but not all, of the observed difference in rate.

The above analysis suggests, by a process of exclusion, the existence of a non-zero inner-sphere reorganizational barrier term for Au_{38} MPC electron transfers. Considering a variety of observations suggesting the importance of polarization of the Au−S bond in Au_{38} behavior, including inductive effects on $Au_{38}^{+/0}$ formal potentials[46] and substituent effects on ligand exchange rates,[47] the idea of a Au−S bond lengthening as a part of the $Au_{38}^{+/0}$ reaction is entirely plausible. However, direct evidence, such as a change in the Au−S vibrational energy, is lacking at present, so this idea must remain as a speculation. Also, since the typical Au−S bond stretching energy (∼2.6 kJ/mol) is similar to k_BT (2.5 kJ/mol, where k_B is the Boltzmann constant and *T* temperature) at 303 K, the Au_{38} MPC system may not be completely in the high-temperature limit. Literature values for vibrational frequencies of Au−S bond stretching in various systems are 230 cm^{-1} (gold nanoparticles passivated by $H_{21}C_{10}SC_{10}H_{21}$)[48] and ∼220 cm^{-1} (alkanethiol self-assembled monolayers on the gold substrate).[49−53]

σ_{EL} and E_A of Nearly Monovalent Au_{38} Films. We return to data in Figure 3 and Tables 2 and 3, where the degree of mixed valency is very low, that is, the films are nearly monovalent. The electronic conductivities and electron-transfer energy barriers are notably lower and higher, respectively, in relation to those in MPC films with more substantial mixed valency. This is emphasized by data in Table 4 for films prepared from Au_{38} MPC solutions having $E_R = -0.47$, −0.17, and 0.11 V, which are nearly monovalent films of Au_{38}^0, Au_{38}^+, and Au_{38}^{2+}, respectively. The conductivities of these films are low, as compared to those of the $Au_{38}^{+/0}$ mixed-valent films,

(39) Holmline, R. E.; Ismagilov, R. F.; Haag, R.; Mujica, V.; Ratner, M. A.; Rampi, M. A.; Whitesides, G. M. *Angew. Chem., Int. Ed.* **2001**, *40*, 2316.
(40) Slowinsky, K.; Majda, M. *J. Electroanal. Chem.* **2000**, *491*, 139.
(41) Häberlen, O. D.; Chung, S.-C.; Stener, M.; Rösch, N. *J. Chem. Phys.* **1997**, *106*, 5189.
(42) Barnett, R. N.; Cleveland, C. L.; Häkkinen, H.; Luedtke, W. D.; Yannouleas, C.; Landman, U. *Eur. Phys. J. D* **1999**, *9*, 95.
(43) Häkkinen, H.; Barnett, R. N.; Landman, U. *Phys. Rev. Lett.* **1999**, *82*, 3264.
(44) (a) Sutin, N. *Acc. Chem. Res.* **1982**, *15*, 275. (b) Sutin. N. *Prog. Inorg. Chem.* **1983**, *30*, 441.
(45) (a) Long, J. W.; Velazquez, C. S.; Murray, R. W. *J. Phys. Chem.* **1996**, *100*, 5492. (b) Williams, M. E.; Masui, H.; Long, J. W.; Malik, J.; Murray, R. W. *J. Am. Chem. Soc.* **1997**, *119*, 1997. (c) Long, J. W.; Kim, I. K.; Murray, R. W. *J. Am. Chem. Soc.* **1997**, *119*, 11510. (d) Kulesza, P. J.; Dickinson, E.; Williams, M. E.; Hendrickson, S. M.; Malik, M. A.; Miecznikowski, K.; Murray, R. W. *J. Phys. Chem. B* **2001**, *105*, 5833.
(46) Guo, R.; Murray, R. W. *J. Am. Chem. Soc.* **2005**, *127*, 12140.
(47) Guo, R.; Song, Y.; Wang, G.; Murray, R. W. *J. Am. Chem. Soc.* **2005**, *127*, 2752.
(48) Chen, Y.; Palmer, R. E.; Shelley, E. J.; Preece, J. A. *Surf. Sci.* **2002,** *502−503*, 208.
(49) Nuzzo, R. G.; Zegarski, B. R.; Dubois, L. H. *J. Am. Chem. Soc.* **1987**, *109*, 733.
(50) Kato, H. S.; Noh, J.; Hara, M.; Kawai, M. *J. Phys. Chem. B* **2002**, *106*, 9655.
(51) Noh, J.; Kato, H. S.; Kawai, M.; Hara, M. *J. Phys. Chem. B* **2002**, *106*, 13268.
(52) Vilar, M. R.; Lang, P.; Horowitz, C.; Nogues, C.; Jugnet, Y.; Pellegrino, O.; do Rego, A. M. B. *Langmuir* **2003**, *19*, 2649.
(53) Kudelski, A. *Vib. Spectrosc.* **2005**, *39*, 200.

Table 4. σ_{EL}, k_{HOP}, and E_A of Nearly Monovalent Au_{38} Films

	σ_{EL} (Ω^{-1} cm^{-1})	k_{HOP} (s^{-1})[a]	E_A (kJ/mol)
Au_{38}^0	6.1×10^{-9}	1×10^3	47
Au_{38}^+	4.3×10^{-9}	7×10^2	58
Au_{38}^{2+}	3.4×10^{-12}	5×10^{-1}	—[b]

[a] $k_{HOP} = 6RT\sigma_{EL}/10^{-3}F^2\delta^2C$. [b] Could not be estimated due to low σ_{EL}.

because (a) in electron-hopping terms the concentration product $[Au_{38}^+][Au_{38}^0]$ is small and (b) in other language, the concentration of charge carriers is very low. It is notable, however, that for the nearly monovalent forms in Table 2, (a) the Au_{140} films are still $\sim 10^3$- to 10^4-fold more conductive than the Au_{38} films and (b) for both, the energy barrier is much larger than that in the mixed-valent films, which implies that the mechanism(s) by which reacting $Au_{38}^{+/0}$ pairs are generated differs when the degree of mixed valency is low. These changes reflect, at least in part, a more efficient thermal generation of charge carriers in Au_{140} films, as by

$$2Au_x^0 \rightarrow Au_x^+ + Au_x^- \qquad (x = 38 \text{ or } 140) \qquad (10)$$

This disproportionation reaction has, at 30 °C, thermal equilibrium constants of 2×10^{-27} for Au_{38} and 1×10^{-5} for Au_{140}, given the −1.6 and −0.3 V formal potential differences $E^{\circ\prime}(Au_x^{0/-}) - E^{\circ\prime}(Au_x^{0/+})$ for Au_{38} and Au_{140}, respectively. These constant are enormously different; thermal carrier generation in Au_{140} films is inefficient, but in Au_{38} films it is insignificant.

Table 4 further shows that the conductivity of nearly monovalent films tends to decrease in the order of $Au_{38}^0 > Au_{38}^+ \gg Au_{38}^{2+}$. This effect must be regarded as a preliminary result. There may be differences in the degree of mixed valency that contribute to some of the difference, and the stability of the Au_{38}^{2+} material is not as well established.

Acknowledgment. This research was supported in part by grants from the National Science Foundation, the STC Program of the National Science Foundation, and the Office of Naval Research.

Supporting Information Available: Complete ref 12, Au_{38} nanoparticle syntheses, C_{CELL} model discussion, supplementary CV of Au_{38}, UV−vis absorption spectra of Au_{38} films, and Arrhenius plots of nearly monovalent Au_{38}^0 and Au_{38}^+. This material is available free of charge via the Internet at http://pubs.acs.org.

JA062736N